

# Stylized Structural Patterns for Improved Neural Network Pre-training

Farnood Salehi<sup>1\*</sup> Vandit Sharma<sup>2\*</sup> Amirhossein Askari Farsangi<sup>1</sup> Tunç Ozan Aydın<sup>1,2</sup>  
<sup>1</sup>Disney Research | Studios <sup>2</sup>ETH Zürich

## Abstract

Modern deep learning models in computer vision require large datasets of real images, which are difficult to curate and pose privacy and legal concerns, limiting their commercial use. Recent works suggest synthetic data as an alternative, yet models trained with it often underperform. This paper proposes a two-step approach to bridge this gap. First, we propose an improved neural fractal formulation through which we introduce a new class of synthetic data. Second, we propose reverse stylization, a technique that transfers visual features from a small, license-free set of real images onto synthetic datasets, enhancing their effectiveness. We analyze the domain gap between our synthetic datasets and real images using Kernel Inception Distance (KID) and show that our method achieves a significantly lower distributional gap compared to existing synthetic datasets. Furthermore, our experiments across different tasks demonstrate the practical impact of this reduced gap. We show that pretraining the EDM2 diffusion model on our synthetic dataset leads to an 11% reduction in FID during image generation, compared to models trained on existing synthetic datasets, and a 20% decrease in autoencoder reconstruction error, indicating improved performance in data representation. Furthermore, a ViT-S model trained for classification on this synthetic data achieves over a 10% improvement in ImageNet-100 accuracy. Our work opens up exciting possibilities for training practical models when sufficiently large real training sets are not available.

## 1. Introduction

The introduction of the ImageNet dataset [11] was one of the main catalysts for the use of deep learning models in computer vision. Today, most computer vision models rely on extensive collections of real-world image data for training. As model architectures grow in complexity and achieve superior performance, the demand for larger datasets has surged, pushing the boundaries of data collection efforts, which remain challenging and costly. These datasets usually come with concerns related to privacy (e.g., including

sensitive personal information), licensing (e.g., including copyright-protected data), and ethics (e.g., low wages for data labeling workers) in the curation process, making them unsuitable for the production environment.

Recent works have shown that computer generated images, which we call synthetic datasets, can be used to pre-train deep learning models. Several classes of synthetic datasets, such as dynamical systems-based (e.g., FractalDB [18]), noise-based (e.g. statistical noise [4]), and CGI-based (e.g., Shaders [5]), have been proposed for training computer vision models by previous work. With some fine-tuning on a small amount of real data, these datasets lead to significant improvements over training from scratch. However, there still exists a significant difference in the standalone performance of models trained with synthetic datasets vs. real datasets, primarily due to the domain gap between real and synthetic images. Moreover, previous methods have predominantly focused on discriminative tasks. In contrast, we focus on generative tasks, which are crucial for applications such as image synthesis, data augmentation, and representation learning, where high-quality synthetic data can significantly impact downstream performance.

In this work, we tackle this problem by making the following contributions:

1. *Neural Fractals*: We propose an improved formulation of neural fractals, which are derived from dynamical systems based on complex-valued neural networks. Our improved neural fractals outperform previous synthetic datasets on three out of our four evaluation pipelines, contributing to the existing literature on synthetic data for training computer vision models.

2. *Synthetic Dataset Stylization*: In typical image stylization, the contents of real images are combined with the style of an artwork, resulting in images with visual features of the *style image* and the contents of the *content image*. We, however, are interested in creating synthetic images with visual features that resemble real images. To this end we introduce *reverse-stylization*, in which we transfer features from a small sample of license-free real images to synthetic images. We show that a modest dataset of only 7000 real images is sufficient to effectively reverse-stylize

\*Equal contribution.

Train/Eval Data	AutoEncoding↑	ImageGen↑	Domain Gap↓
	ImgNet	ImgNet	KID
VisualAtom	0.28	0.42	0.203
Mandelbulb	0.17	0.35	0.165
FracDB-comp	0.50	0.51	0.214
StGAN-oriented	0.47	0.54	0.170
NeuFractal (ours)	<b>0.55</b>	<b>0.57</b>	<b>0.162</b>
+RevStylize (ours)	<b>0.68</b>	<b>0.61</b>	<b>0.120</b>

Table 1. The first two columns show cosine similarity between attention maps of a network trained on ImageNet-100 and those trained on synthetic datasets. The left column corresponds to an autoencoder [24] trained for image reconstruction, and the middle column to EDM2 [17] trained with a diffusion loss. The rightmost column reports the Kernel Inception Distance (KiD) between each synthetic dataset and ImageNet, measuring distribution-level similarity. Neural fractal achieves the highest cosine similarity and the lowest KiD score, indicating the closest alignment with ImageNet-trained network and the smallest domain gap among all evaluated datasets.

a significantly larger synthetic dataset, leading to improvements in evaluation metrics of up to 20% compared to models trained solely on existing synthetic datasets or limited real data.

3. *Extensive Experimental Evaluation:* We conduct experiments on three tasks: Image Autoencoding, Image Generation, and Representation Learning. Our models trained on reverse-stylized neural fractals outperform those trained on baseline datasets. This improvement can be attributed to the reduced domain gap between our synthetic data and real images. Table 1 highlights this with a lower KID score (third column). KID measures the distribution difference between synthetic and real data (ImageNet). A lower KID score suggests that models trained on our dataset produce feature representations that better align with those from real data (first two columns). Further details of this experiment are provided in the experiments section.

## 2. Related Work

### 2.1. Fractals

Fractals are geometric patterns that exhibit great complexity and self-similarity at different scales. They are found everywhere in nature, from snowflakes to tree leaves [14]. They can also be generated using computer programs using simple rules. Due to these properties, fractals have been investigated by previous works such as Kataoka et al. [18] and Anderson et al. [2] as a potential replacement for real datasets to pre-train vision models.

There is a wide variety of fractals generated by several techniques [29]. The Mandelbrot set [22], defined as complex numbers  $c$  where  $f_c(z) = z^2 + c$  does not diverge from  $z = 0$ , is the most well-known. Its intricate bound-

aries are promising for synthetic data, though zooming in is computationally expensive and often yields featureless areas. Asadi [3] proposed a neural dynamical system for visual fractal exploration, but it faces several challenges that limit its practicality beyond visual curiosity: it uses monochromatic coloring, is slow to render, and requires manual hyperparameter tuning. In contrast, we address these challenges in the context of synthetic data generation, introducing an adaptive rendering technique to improve rendering speed, an escape-time coloring algorithm that produces diverse RGB images, and an algorithm for automatic hyperparameter tuning.

### 2.2. Synthetic Data Pre-training

The idea of using synthetically generated data to train vision models was first explored by Kataoka et al. [18]. They introduced FractalDB, a synthetic dataset consisting of mathematically-generated fractal images, which could outperform ImageNet-1k [11] and Places365 [33] pre-trained models with some fine-tuning. Anderson et al. [2] improved fractal pre-training by proposing a better sampling process for Iterated Function System (IFS) codes leading to higher quality fractal images. Nakashima et al. [23] demonstrated the effectiveness of FractalDB to pre-train Vision Transformers [12], or ViTs, and observed that ViTs pay attention to contour lines in the pre-training phase. Subsequently, works such as Kataoka et al. [19] and Takashima et al. [28] explored contour-based datasets built using overlapping polygons (RCDB) and sinusoidal waves (VisualAtom) respectively, the latter achieving state-of-the-art fine-tuning performance. Unlike our method, FractalDB and VisualAtom is designed for supervised training. Shinoda et al. [27] extended the concept of synthetic pre-training from classification to semantic segmentation, and introduced the SegRCDB dataset with automatically-generated segmentation labels. Baradad et al. [4] investigated if images generated from procedural noise processes could suffice to train vision models. They experimented with several models (procedural graphics, statistical, StyleGAN initializations, etc.) and concluded that models trained on structured noise could indeed learn meaningful features. Baradad et al. [5] curated a large collection of OpenGL shaders to generate a diverse and effective procedural graphics-based dataset of synthetic images.

Using synthetic data comes with several advantages: 1. It is free from privacy, ethical, and legal issues, 2. Data labelling can be performed cheaply and accurately, 3. It can be generated in large quantities without significant human effort, and 4. It is quite effective for pre-training vision models. However, existing synthetic datasets still perform significantly worse than real-world datasets, particularly for image generation tasks such as image autoencoding and image diffusion. Our work aims to narrow this gap.

### 2.3. Neural Style Transfer

Neural Style Transfer (NST) is a Deep Learning-based technique that allows an ordinary image (*content* image) to be generated in the style of an artistic image (*style* image). While image stylization has been a long-standing field of research, the use of deep neural networks to transfer artistic style across images was first proposed by Gatys et al. [13]. Their approach uses a bipartite loss function to optimize the resulting image. The first part (*content* loss) aimed to preserve content features with respect to the *content* image, and is derived using higher layers from a CNN network. The second part (*style* loss), is responsible for preserving style features with respect to the *style* image, which are modelled using Gram matrices derived from feature representations at intermediate CNN layers. The authors showed that such *content* and *style* representations are separable, thus allowing the generation of images that combine traits of both *content* and *style* images using optimization.

Since then, NST has gained tremendous popularity. It has been expanded to various domains Cai et al. [8] and several new approaches have been proposed. Jing et al. [16] conducted a literature review of the advances in this area and performed a qualitative and quantitative comparison of various approaches. Kolkin et al. [20] proposed the Neural Neighbor Style Transfer (NNST) approach using nearest-neighbour matching to replace neural features in the *content* image with ones from the *style* image, resulting in high-quality stylized images. More recently with the Generative AI wave, several diffusion-based [24] techniques [15, 25, 32] have also been proposed. In this work, we restrict ourselves to two texture-based style transfer methods: Gatys et al. [13] and Kolkin et al. [20].

### 3. Methodology

We propose a novel two-step approach to generate high-quality synthetic data for training neural networks for a wide variety of computer vision tasks. The first step involves generating a base synthetic dataset. Here, we propose an improved formulation of neural fractals as a new type of synthetic data. These are fractal patterns generated using dynamical systems defined by complex-valued neural networks. The second step involves stylizing the base synthetic dataset using a small sample of real images. We show that this step helps boost the dataset quality tremendously as it incorporates real image features while retaining properties of the base synthetic dataset.

#### 3.1. Neural Fractal Generation

We explore neural fractals as a potential alternative to the Mandelbrot set limitations described in Section 2.1. Neural fractals are derived from the following generalization of the

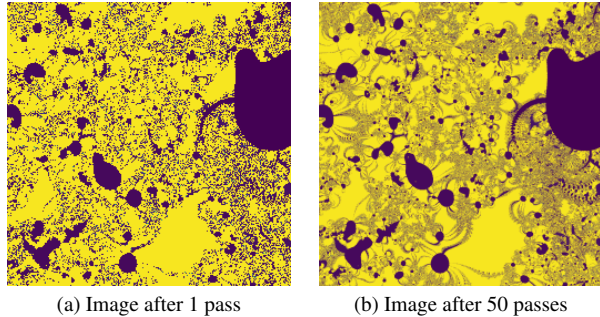


Figure 1. Rendering the neural fractal is a noisy process.

original Mandelbrot recurrence relation:

$$z_{n+1} = g(z_n) + c, \quad z_0 = 0, \quad (1)$$

where  $c = x + y \cdot j \in \mathbb{C}$  represents the continuous 2D coordinate  $(x, y)$  in the image plane as a complex number. In the case of the Mandelbrot set,  $g(z) = z^2$ . However, in principle,  $g$  can be extended to any real or complex-valued function. Neural fractals use a randomly initialized complex-valued neural network as  $g$ . To determine whether a coordinate  $c = x + y \cdot j$  belongs to the fractal set, the recurrence relation in Equation 1 is iterated for a fixed number of iterations  $T$  to obtain  $z_T(c)$ . Points for which  $z_T(c)$  remains bounded (i.e.,  $|z_T(c)| \leq \tau$  where  $\tau$  is the threshold) belong to the fractal set. To rasterize the final image, we integrate over each pixel  $P$  by computing

$$\int_{(x,y) \in P} 1_{\{|z_T(x + y \cdot j)| \leq \tau\}} dx dy. \quad (2)$$

Similar to [3], our implementation works as follows: To compute the integral in Equation 2, we use Monte Carlo estimation. At the start of each epoch, a subset of points  $\{c_0, \dots, c_n\}$  is uniformly sampled from the available image plane (a pre-determined rectangular window in the complex plane based on the center’s coordinates). Next, we compute  $z_T(c_i) \forall i$  by iteratively applying Equation 1. At the end of this iterative process, the pixel value is determined by counting the number of  $c_i$ s within the pixel for which  $|z_T(c_i)|$  remains within the threshold  $\tau$ .

Note that this process is inherently noisy, as different points landing in a pixel can have different locations and subsequently different values (see Figure 1). To mitigate this noise, the rendering process is repeated over several passes, allowing each pixel to converge to its final value. After completing all passes, the intensity of each pixel in the final image is determined by averaging the results across all passes. This procedure results in a grayscale image by default, which is then colorized, whereby pixel intensities are mapped to colors using a color map that we discuss next.

Each random initialization of the network weights results in a unique and complex recurrence relation, rendering a

completely unique fractal image. Since neural fractals derive variations in the fractal pattern from the random initialization of network weights and not the zoom location or level, they offer a practical way to generate practically infinite, diverse fractal patterns. We use a fully connected neural network with 6 hidden layers of 3 neurons each, with complex weights drawn from a normal distribution. The network uses tanh activation, and the output of the network is raised to the third power. In later sections, we show that this process generates meaningful fractal images that perform well for training vision models.

**Selecting  $\tau$  in Equation 2** We choose  $\tau$  in Equation 2 to ensure the rendered fractal exhibits intricate structure and visual richness. If  $\tau$  is too small or too large, the image becomes entirely black or white, respectively. Complicating the selection, the optimal  $\tau$  depends on the neural network  $g$ , which varies for each fractal. To address this, we employ an automatic adjustment process: after an initial rendering pass and obtaining values  $|z|$ , starting from a small initial value  $\tau$  is iteratively increased by a factor of 1.1 until at least 40% of the rendered values  $|z|$  fall below the threshold. The remaining rendering process then uses this adjusted  $\tau$ , ensuring a well-balanced distribution of values, preserving structural detail. For completeness, we provide the algorithm in the Appendix.

**Escape Time Coloring** We adopt escape-time algorithm [22], in which we keep track of *escape count*, i.e. the number of iterations required for each sampled point to escape the threshold  $\tau$ . All points that escape the dynamical system with the same escape count (i.e. in a particular iteration) are then assigned the same color sampled randomly from a color map. Consequently, the pixels corresponding to these escaped points also hold the same color given the one-to-one mapping. Once a point escapes, its pixel color is frozen, and subsequent iterations are used to colorize only the remaining pixels. The final image is formed by averaging the intermediate images across all passes. Escape-time coloring reveals underlying patterns that are not captured by pseudo-coloring scheme proposed in [3]. Figure 2 compares the two coloring algorithms. A colored dataset is crucial for applications such as image autoencoding and image generation pretraining. We provide the full coloring algorithm in the Appendix.

**Adaptive Sampling** Second, we tackle the issue of slow rendering, which arises from the naive sampling of the image plane. This naive approach requires a large number of iterations to remove noise and achieve a final high-quality fractal. Inspired by adaptive sampling techniques in Monte Carlo rendering [7], we introduce an adaptive sampling of

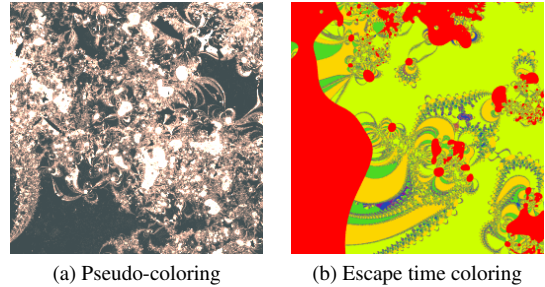


Figure 2. Pseudo-coloring vs Escape time coloring.

query points, which significantly accelerates the neural fractal generation process. Rather than uniformly sampling points across the entire image plane, adaptive sampling allocates samples nonuniformly according to the rendering difficulty of each pixel. By selectively avoiding sampling pixels that are easy to render, this approach reduces computational costs and accelerates rendering.

In a first pass, we distribute a few samples uniformly per pixel and render their corresponding color. We calculate the variance of these rendered colors for each pixel and smoothen the resulting variance map with a box filter using a kernel of size 5. This smoothed map is normalized and serves as a sampling map to allocate the samples in the next step. After each pass, we update the variance map and adjust the sampling distribution accordingly. Our experiments show that adaptive sampling can increase rendering speed on average by a factor of 8 and produce visually noiseless images. Using a single RTX 3090 GPU, generating an image takes on average about 6 seconds. Figure 3 shows an example of the estimated variance and the rendered image. As is seen, the variance is very low across large portions of the image, allowing them to be rendered with a small number of samples. Our adaptive sampling algorithm reduces the sample density in these areas. We also add a stopping criterion to prevent distributing samples to a pixel if its estimated variance is below a certain threshold. Adaptive sampling does not alter image content; it only accelerates the rendering process. Figure 4 shows the complete neural fractal generation process. For details on the adaptive sampling algorithm, please refer to the Appendix.

Similar to Baradad et al. [4], we generate a total of 100K,  $256 \times 256$ , random neural fractal images to use as our base synthetic dataset. For each image, we re-initialize the MLP network  $g$  with random weights. To prevent featureless images from being included in the dataset, we exclude all generated image samples having a maximum standard deviation less than 0.025 across any channel.

As baselines, we use several synthetic datasets such as StyleGAN-oriented [4], FractalDB-composite [2], VisualAtom [28], and Mandelbulb [10], which have been shown to perform well for synthetic data training in prior work. We



Figure 3. Adaptive sampling. As shown in the estimated variance, certain pixels converge more quickly and require fewer samples.

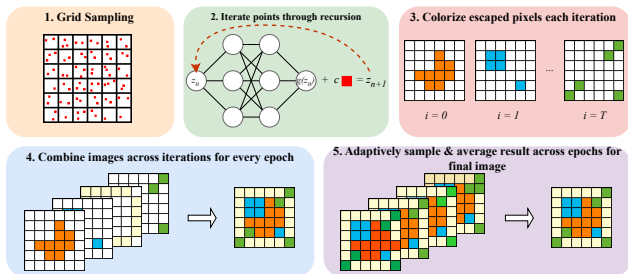


Figure 4. Overview of the neural fractal generation process.

generate 100K,  $256 \times 256$ , samples for each dataset using the original code provided by the authors. Samples from all base datasets have been provided in Figure 9 in Appendix.

Notably, networks trained on neural fractal exhibit a smaller domain gap than those trained on other synthetic datasets. As shown in the first two columns of Table 1, the attention map of a network trained on neural Fractal aligns more closely with that of a network trained on ImageNet, as measured by cosine similarity. This alignment is further supported by the lower KID score in the third column, indicating reduced distributional discrepancy. The complete set of neural fractal experiments is in subsection 4.1.

### 3.2. Neural Fractal Reverse-stylization

Previous works [4, 18] in the direction of synthetic pre-training have revealed that there still exists a large gap between the performance of models trained on synthetic data compared to real data such as ImageNet [11]. We also experience this effect first hand when training purely on neural fractals mentioned above. We believe that one shortcoming of synthetic data is the lack of realistic textures and an inaccurate color distribution, which may contribute to this performance gap. In order to bridge this gap, we look into neural stylization of synthetic datasets as a way to boost their performance.

Neural style transfer is typically used in the setting of artistic image generation, where the contents of a photograph are combined with the style of an artwork. This results in an image with visual features of the style image,



Figure 5. Samples from our *Unsplash* dataset.

but overall contents of the content image. We, however, are interested in creating synthetic datasets with visual features that resemble real datasets, to bridge the domain gap. We do this by running neural style transfer in the opposite direction, allowing the visual features of a real image to be transferred to a synthetic image.

To demonstrate our approach, we collect a small dataset of around 7k, real-world, license-free images, by scraping the website Unsplash<sup>1</sup>. We downsize the images to  $256 \times 256$  for our use case. We refer to the resulting dataset as *Unsplash* (Figure 5), and use it for stylization as well as the real data baseline in our experiments. Unlike large-scale datasets such as ImageNet, collecting a small dataset requires significantly less manpower, and can be manually verified to be free of legal or privacy issues. Next, we select a base synthetic dataset to be stylized. Here, we experiment and report results using our own neural fractal dataset, as well as other synthetic datasets. To generate style-transferred synthetic datasets, we iterate through each sample in a base synthetic dataset, and stylize it using a randomly sampled real image from the *Unsplash* dataset. We experiment with two texture-based neural style transfer algorithms: The original algorithm by Gatys et al. [13], and the NNST method proposed later by Kolkin et al. [20].

Using this procedure, we generate generate 100K,  $256 \times 256$ , samples for each combination of base synthetic dataset and stylization algorithm. Figure 6 show samples from all stylized synthetic datasets using NNST stylization algorithms, samples from Gatys stylized method are shown in Appendix (Figure 10). Note that both stylization algorithms originally use features derived from a VGG network (trained on ImageNet). Therefore, we replace it with an encoder network pre-trained on *Unsplash* to prevent any biases in results arising from using a network trained on large-scale real data. Based on our testing, the results from either yield visually very similar results.

Table 1 shows that reverse stylization reduces the domain gap significantly, as evidenced by both the improved alignment of attention maps with the ImageNet-trained network and the lower KID score, indicating closer distribu-

<sup>1</sup><https://unsplash.com/>

Train/Eval dataset	ImgNet	COCO
ImageNet-100	0.090	0.074
<i>Unsplash</i>	0.153	0.121
VisualAtom	0.320	0.303
Mandelbulb	0.616	0.506
FractalDB-composite	0.224	0.195
StyleGAN-oriented	0.138	<b>0.114</b>
Neural Fractals	<b>0.137</b>	0.116

Table 2. Reconstruction loss of autoencoder networks trained on different Train datasets and evaluated on ImgNet and COCO validation datasets.

tional similarity. Details on reverse stylization experiments are provided in [subsection 4.2](#).

## 4. Experiments

We conduct experiments to test the quality of our synthetic datasets using three evaluation pipelines. In [subsection 4.1](#), we compare the performance of neural fractals against other synthetic datasets proposed in previous works. Then, in [subsection 4.2](#), we conduct experiments for our stylized synthetic dataset. Finally, we present ablation studies to gain a better understanding of the effect of different parameters.

### 4.1. Training with Neural Fractals

**Autoencoder:** We begin by training an autoencoder network designed for perceptual compression using an implementation and hyperparameters similar to Rombach et al. [24]. We train solely using the perceptual loss [31] and disable the adversarial objective (implemented for local realism) to avoid domain gap issues. We train on synthetic datasets and test on ImageNet’s and COCO’s [21] validation dataset. We choose this network for its high reconstruction quality. Training hyperparameters are provided in the Appendix. Importantly, we also use its encoder as a VGG replacement to generate features for style transfer. We train the network for 1M iterations.

[Table 2](#) shows the final reconstruction loss for different testing datasets. As can be seen, neural fractals and StyleGAN-oriented performs the best among all synthetic datasets.

**Diffusion:** To evaluate our approach in image generation tasks, we experiment with diffusion models, using the EDM2 framework [17]. We adopt a network architecture based on the EDM2 repository, following their design guidelines. Similar to [17], we downscale the images to a resolution of 64 and train the diffusion model in image space. Full network and training hyperparameters are provided in the Appendix. After pretraining the model on synthetic datasets, the network is fine-tuned on two small datasets, Flowers (8K images) and FFHQ (70K images). We follow the standard FID computation procedure in [17]

Pretrain/Target dataset	Flowers	FFHQ
ImageNet-100	10.2	7.2
<i>Unsplash</i>	29.0	9.1
VisualAtom	43.1	8.3
Mandelbulb	28.8	8.5
FractalDB-composite	18.9	8.4
StyleGAN-oriented	20.1	8.1
Neural Fractals	<b>18.3</b>	<b>7.4</b>

Table 3. FID measured after pretraining with pretrain data and fine-tuning on the target dataset.

Dataset	ImgNet100	Flowers	Food101
ImageNet-100	78.2	75.6	64.8
<i>Unsplash</i>	44.8	47.8	38.5
VisualAtom	38.9	36.4	24.7
Mandelbulb	44.0	50.15	41.0
FractalDB-composite	45.3	55.6	37.4
StyleGAN-oriented	48.1	59.9	45.4
<b>Neural Fractals</b>	<b>48.5</b>	<b>60.6</b>	<b>49.8</b>

(a) Results with a single linear classifier on frozen features.

Dataset	ImgNet100	Flowers	Food101
ImageNet-100	70.7	80.3	67.1
<i>Unsplash</i>	-	-	-
VisualAtom	44.2	42.6	30.7
Mandelbulb	48.5	55.1	45.2
FractalDB-composite	48.3	59.5	40.9
StyleGAN-oriented	51.5	63.5	48.9
<b>Neural Fractals</b>	<b>56.3</b>	<b>65.6</b>	<b>55.1</b>

(b) Results using an MLP head with linear, batch normalization, ReLU, and another linear layer on frozen features.

Table 4. Top-1 accuracy on ImageNet-100, Flowers, and Food101 after training an encoder on synthetic data using the DINO pipeline, followed by training with different classifier head configurations on the respective datasets.

with 50K generated images and apply the independent condition guidance method from [26] to generate the images. [Table 3](#) shows the results. Neural fractals perform the best among all synthetic datasets.

#### Contrastive Learning:

Inspired by the contrastive learning-based evaluation pipeline from [5], we use DINO [9] with a ViT-S backbone. DINO is pre-trained self-supervised with a contrastive loss on synthetic datasets, and we train only a linear classifier on the frozen features to evaluate representation quality—unlike [10, 28], which use fully supervised training of the entire network. We train the encoder for 1000 epochs before adding the linear classifier on top.

[Table 4](#) (a) shows the top-1 accuracy achieved by different datasets for our contrastive learning pipeline. Neural fractals achieve the highest accuracy across all validation datasets. For completeness, we also tried a larger classifier head consisting of a linear layer, batch normalization, ReLU, and another linear layer. This setup also yielded the



Figure 6. Samples from different *NNST*-stylized synthetic datasets.

same result: neural fractals achieved the best performance.

## 4.2. Training with Reverse Stylized Neural Fractals

In this section, we evaluate the effectiveness of reverse stylization in enhancing network performance. We use algorithms similar to *NNST* and *Gatys*. For brevity, we refer to these simply as *NNST* and *Gatys*. Both stylization algorithms significantly improve the quality of neural fractals.

**Autoencoder:** The first set of results in Table 5 presents the final reconstruction loss for an autoencoder trained on *reverse-stylized Neural Fractals* dataset and tested on ImageNet-100 and COCO. Stylization reduces the loss by approximately 20% compared to the non-stylized dataset, while *Gatys* outperform *NNST*.

**Diffusion:** We pretrain the network with *reverse-stylized Neural Fractals* and finetune it on the Flowers and FFHQ datasets. We only use *NNST* stylization in this section. The second set of results in Table 5 shows the FID reduction achieved through stylization. On Flowers, stylization reduces FID by 11%, while on FFHQ, it achieves a 1% reduction. An uncurated selection of generated images is provided in the Appendix.

**Contrastive Learning:** The third set of results in Table 5 shows the top-1 accuracy on ImageNet-100 and Flowers achieved by *reverse-stylized Neural Fractals* using the DINO-based contrastive learning pipeline. Reverse stylization of the neural fractals significantly improves accuracy. *NNST* outperforms *Gatys* in representation learning tasks.

In Appendix, we show that reverse stylization is effective not only for neural fractals but also consistently improves all other synthetic datasets. This suggests that reverse styliza-

tion can be a general technique for enhancing synthetic data across various applications. Figure 7 summarizes the performance of our approach for the three evaluation pipelines. Figures 11 and 12 (Appendix) contain a more detailed performance comparison.

## 4.3. Ablation Studies

**Domain Gap:** We analyze the domain gap between our *reverse-stylized Neural Fractals* and real data. To quantify this gap, we compute the Kernel Inception Distance (KID) [6] between each synthetic dataset and ImageNet. We choose KID over FID due to its unbiased estimation and ability to report confidence intervals, which makes it more robust—particularly in high-divergence regimes. As shown in the third column of Table 1, the neural fractal dataset achieves the lowest KID with respect to ImageNet, indicating the closest distributional match. This gap is further reduced through our reverse stylization step, highlighting its effectiveness in aligning the synthetic data distribution with that of real images. For completeness, we report FID values in Appendix, which support the same conclusion. Beyond distributional similarity, we further analyze the behavior of networks trained on different datasets. Specifically, we compare attention maps produced by autoencoders and diffusion models using ImageNet-100k trained-network as a reference. We calculate the cosine similarity between the attention maps of networks trained on synthetic datasets and those trained on ImageNet. Higher similarity indicates closer alignment in attended regions. Our method consistently achieves the highest similarity scores, as shown in Table 1, and is further supported by visualizations in Fig-

Dataset	AutoEncoding↓		ImageGen↓		Representation Learning↑		
	ImgNet	COCO	Flowers	FFHQ	ImgNet	Flowers	Food101
Neural Fractals	0.137	0.116	18.3	7.4	48.5	60.6	49.8
+RevStyl NNST	0.111 +19%	0.088 +24%	<b>16.3</b> +11%	<b>7.3</b> +1%	<b>59.2</b> +10.7%	<b>71.3</b> +10.7%	<b>55.0</b> +5.2%
+RevStyl Gatys	<b>0.105</b> +23%	<b>0.084</b> +28%	-	-	57.4 +8.9%	68.7 +8.1%	53.9 +4.1%

Table 5. Performance comparison of *reverse-stylized Neural Fractals* in autoencoding, diffusion-based generation and representation learning, using *NNST* and *Gatys* for stylization. Improvement is computed as  $100 \times \frac{\text{NeuralFractal} - \text{RevStylNeuralFractal}}{\text{NeuralFractal}}$  for generation tasks and as  $\text{RevStylNeuralFractal} - \text{NeuralFractal}$  for representation learning.

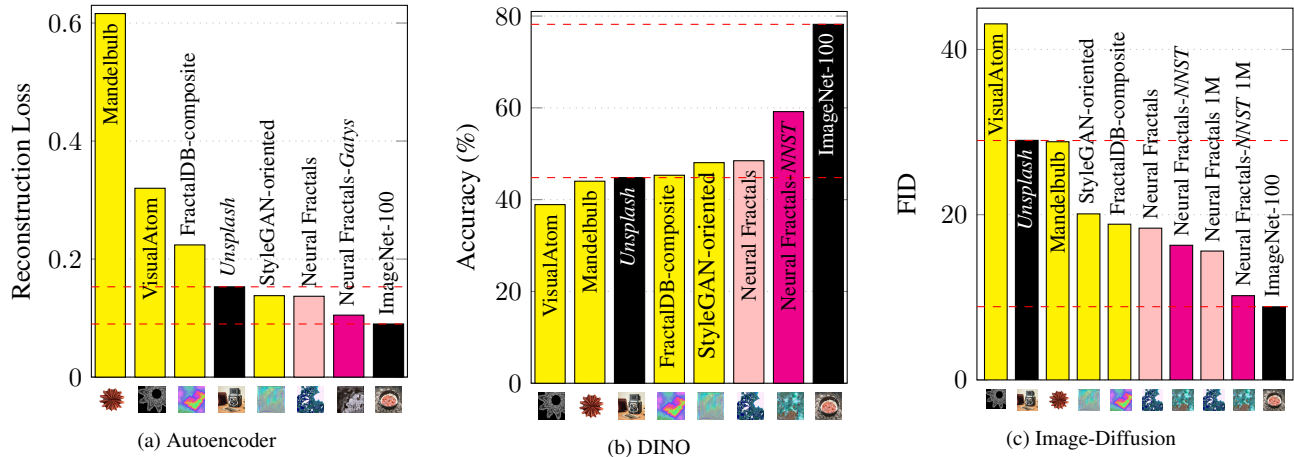


Figure 7. Dataset performance across evaluation pipelines. Most datasets have 100K images, except two with 1M in image-diffusion. Stylized synthetic datasets perform best. ImageNet is used for (a) and (b), Flowers for (c).

Figure 18 (autoencoder attention maps) and Figure 17 (latent visualizations) in the Appendix. These results suggest a reduced domain gap compared to other synthetic datasets.

**Impact of Dataset Scaling:** In the diffusion experiment, we studied the effect of dataset scaling by generating 1 million images from an expanded neural fractals dataset and its stylized counterpart. We trained separate networks on each dataset and fine-tuned them on Flowers and FFHQ. Increasing dataset size reduced FID by approximately 15% for the non-stylized version and 30% for the reverse-stylized version (Table 6).

Dataset	Flowers	FFHQ
nFractal 100K	18.4	7.4
nFractal 1M	<b>15.6</b>	<b>6.5</b>
+ RevStyle 100K	16.3	7.3
+ RevStyle 1M	<b>10.2</b>	<b>5.5</b>

Table 6. Effect of dataset size on diffusion: Larger data improves FID for (non-)stylized neural fractal trained networks.

**Effect of style algorithm:** Comparing results be-

tween *Gatys* and *NNST* stylized datasets, we notice that *NNST* tends to perform better on contrastive learning tasks, whereas *Gatys* has a slight edge in the autoencoder setting. See Table 8 and Table 9 in Appendix.

#### Impact of Network Architecture on Neural Fractals:

We explore network complexity in neural fractals generation. We observe that networks with more layers (see section 9 in Appendix) are more likely to produce images with rich high-frequency details, while on the other hand making rendering harder and network calls slower. To balance speed and detail, we use a 3-layer, 6-neuron network.

**Comparison to MixUp:** MixUp [30] is a data augmentation technique that blends two input samples to improve model generalization. We compare Mixup with reverse stylization in Table 7 and find that reverse stylization performs significantly better.

## 5. Discussion & Limitations

We showed that stylizing existing synthetic datasets with features from a small sample of real images greatly improves performance. Our reverse-stylization approach transfers visual features from real data to synthetic data, re-

Dataset / Method	DINO $\uparrow$	AEncoder $\downarrow$
nFractal	<u>48.5</u>	0.137
+ MixUp	45.0	<u>0.128</u>
+ RevStylize	<b>59.2</b>	<b>0.105</b>

Table 7. Comparison of MixUp and reverse stylization on DINO feature quality and Autoencoder reconstruction loss both on ImageNet. Higher DINO scores indicate better representation learning, while lower Autoencoder loss (AEncoder) indicates better reconstruction.

ducing the domain gap. Our approach has some limitations. First, for generating neural fractals, we restricted ourselves to a simple MLP architecture to model  $g$  in recurrence relation 1. However, it is likely that other model architectures can generate different or more sophisticated patterns. Perhaps, this is something that could be used to generate labeled neural fractal datasets for classification tasks. In terms of stylization, we relied on a small sample of real images to transfer features to synthetic datasets. The exact effect of this real dataset on final results is not clear at the moment. Jing et al. [16] highlighted that there exist several stylization algorithms that can run in real time. However, this was not the focus of our work and can be explored in future studies.

## 6. Conclusion

In this work, we explored using synthetic data to train deep learning-based computer vision models. We proposed an improved version of neural fractals—a new class of synthetic training data derived from dynamical systems using complex-valued neural networks. Training models with neural fractals achieved the best performance across our synthetic dataset evaluation pipelines. To further boost performance, we introduced a technique involving neural stylization of synthetic datasets with a small sample of real images as a way of reducing the domain gap and adding meaningful features to synthetic data. The resulting stylized synthetic datasets achieved superior performance: up to 24% for Autoencoder, 11% for the DINO-based and 11% for the diffusion evaluation pipelines. Stylization especially benefited weaker base synthetic datasets, with all stylized datasets managing to outperform the best synthetic data baseline. We believe our work will find applications in data-scarce settings, and hope that our strong results will pave the way for future research.

## References

[1] Stability AI. Autoencoder configuration file (kl-f4), 2023. Accessed: Nov. 15, 2024. 11

[2] Connor Anderson and Ryan Farrell. Improving fractal pre-training. In *Proceedings of the IEEE/CVF Winter Confer-*

*ence on Applications of Computer Vision*, pages 1300–1309, 2022. 2, 4

[3] Amirabbas Asadi. Neuralfractal - a visual exploration of neural dynamical systems. <https://amirabbasasadi.github.io/neural-fractal/>, 2021. (Last accessed on September 2024). 2, 3, 4

[4] Manel Baradad, Jonas Wulff, Tongzhou Wang, Phillip Isola, and Antonio Torralba. Learning to see by looking at noise. In *Advances in Neural Information Processing Systems*, 2021. 1, 2, 4, 5

[5] Manel Baradad, Richard Chen, Jonas Wulff, Tongzhou Wang, Rogerio Feris, Antonio Torralba, and Phillip Isola. Procedural image programs for representation learning. *Advances in Neural Information Processing Systems*, 35:6450–6462, 2022. 1, 2, 6

[6] Mikołaj Bińkowski, Danica J Sutherland, Michael Arbel, and Arthur Gretton. Demystifying mmd gans. *arXiv preprint arXiv:1801.01401*, 2018. 7

[7] Brent Burley, Yining Karl Li, Felix Hecht, Bruce Meyer, and Matthew Hill. The design and evolution of disney’s hyperion renderer. *ACM Transactions on Graphics (TOG)*, 37(3):1–22, 2018. 4

[8] Qiang Cai, Mengxu Ma, Chen Wang, and Haisheng Li. Image neural style transfer: A review. *Computers and Electrical Engineering*, 108:108723, 2023. 3

[9] Mathilde Caron, Hugo Touvron, Ishan Misra, Hervé Jégou, Julien Mairal, Piotr Bojanowski, and Armand Joulin. Emerging properties in self-supervised vision transformers. In *Proceedings of the IEEE/CVF international conference on computer vision*, pages 9650–9660, 2021. 6, 12

[10] Benjamin Naoto Chiche, Yuto Horikawa, and Ryo Fujita. Pre-training vision models with mandelbulb variations. In *Proceedings of the IEEE/CVF Conference on Computer Vision and Pattern Recognition*, pages 22062–22071, 2024. 4, 6

[11] Jia Deng, Wei Dong, Richard Socher, Li-Jia Li, Kai Li, and Li Fei-Fei. Imagenet: A large-scale hierarchical image database. In *2009 IEEE conference on computer vision and pattern recognition*, pages 248–255. Ieee, 2009. 1, 2, 5

[12] Alexey Dosovitskiy, Lucas Beyer, Alexander Kolesnikov, Dirk Weissenborn, Xiaohua Zhai, Thomas Unterthiner, Mostafa Dehghani, Matthias Minderer, Georg Heigold, Sylvain Gelly, et al. An image is worth 16x16 words: Transformers for image recognition at scale. *arXiv preprint arXiv:2010.11929*, 2020. 2

[13] Leon A Gatys, Alexander S Ecker, and Matthias Bethge. A neural algorithm of artistic style. *arXiv preprint arXiv:1508.06576*, 2015. 3, 5

[14] Shea Gunther. 9 amazing fractals found in nature. <https://www.treehugger.com/amazing-fractals-found-in-nature-4868776>, 2024. (Last accessed on September 2024). 2

[15] Mark Hamazaspyan and Shant Navasardyan. Diffusion-enhanced patchmatch: A framework for arbitrary style transfer with diffusion models. In *Proceedings of the IEEE/CVF Conference on Computer Vision and Pattern Recognition*, pages 797–805, 2023. 3

- [16] Yongcheng Jing, Yezhou Yang, Zunlei Feng, Jingwen Ye, Yizhou Yu, and Mingli Song. Neural style transfer: A review. *IEEE transactions on visualization and computer graphics*, 26(11):3365–3385, 2019. 3, 9
- [17] Tero Karras, Miika Aittala, Jaakko Lehtinen, Janne Hellsten, Timo Aila, and Samuli Laine. Analyzing and improving the training dynamics of diffusion models. In *Proceedings of the IEEE/CVF Conference on Computer Vision and Pattern Recognition*, pages 24174–24184, 2024. 2, 6, 11, 12, 15
- [18] Hirokatsu Kataoka, Kazushige Okayasu, Asato Matsumoto, Eisuke Yamagata, Ryosuke Yamada, Nakamasa Inoue, Akio Nakamura, and Yutaka Satoh. Pre-training without natural images. In *Proceedings of the Asian Conference on Computer Vision*, 2020. 1, 2, 5
- [19] Hirokatsu Kataoka, Ryo Hayamizu, Ryosuke Yamada, Kodai Nakashima, Sora Takashima, Xinyu Zhang, Edgar Josafat Martinez-Noriega, Nakamasa Inoue, and Rio Yokota. Replacing labeled real-image datasets with auto-generated contours. In *Proceedings of the IEEE/CVF Conference on Computer Vision and Pattern Recognition*, pages 21232–21241, 2022. 2
- [20] Nicholas Kolkin, Michal Kucera, Sylvain Paris, Daniel Sykora, Eli Shechtman, and Greg Shakhnarovich. Neural neighbor style transfer. *arXiv e-prints*, pages arXiv–2203, 2022. 3, 5
- [21] Tsung-Yi Lin, Michael Maire, Serge Belongie, Lubomir Bourdev, Ross Girshick, James Hays, Pietro Perona, Deva Ramanan, Piotr Dollár, and C Lawrence Zitnick. Microsoft coco: Common objects in context. *arXiv preprint arXiv:1405.0312*, 2014. 6
- [22] Benoit B Mandelbrot. The fractal geometry of nature/ revised and enlarged edition. *New York*, 1983. 2, 4
- [23] Kodai Nakashima, Hirokatsu Kataoka, Asato Matsumoto, Kenji Iwata, Nakamasa Inoue, and Yutaka Satoh. Can vision transformers learn without natural images? In *Proceedings of the AAAI Conference on Artificial Intelligence*, pages 1990–1998, 2022. 2
- [24] Robin Rombach, Andreas Blattmann, Dominik Lorenz, Patrick Esser, and Björn Ommer. High-resolution image synthesis with latent diffusion models. In *Proceedings of the IEEE/CVF conference on computer vision and pattern recognition*, pages 10684–10695, 2022. 2, 3, 6, 15
- [25] Dan Ruta, Gemma Canet Tarrés, Andrew Gilbert, Eli Shechtman, Nicholas Kolkin, and John Collomosse. Diff-nst: Diffusion interleaving for deformable neural style transfer. *arXiv preprint arXiv:2307.04157*, 2023. 3
- [26] Seyedmorteza Sadat, Manuel Kansy, Otmar Hilliges, and Romann M Weber. No training, no problem: Rethinking classifier-free guidance for diffusion models. *arXiv preprint arXiv:2407.02687*, 2024. 6
- [27] Risa Shinoda, Ryo Hayamizu, Kodai Nakashima, Nakamasa Inoue, Rio Yokota, and Hirokatsu Kataoka. Segrcdb: Semantic segmentation via formula-driven supervised learning. In *Proceedings of the IEEE/CVF International Conference on Computer Vision*, pages 20054–20063, 2023. 2
- [28] Sora Takashima, Ryo Hayamizu, Nakamasa Inoue, Hirokatsu Kataoka, and Rio Yokota. Visual atoms: Pre-training vision transformers with sinusoidal waves. In *Proceedings of the IEEE/CVF Conference on Computer Vision and Pattern Recognition*, pages 18579–18588, 2023. 2, 4, 6, 16
- [29] Wikipedia contributors. Common techniques for generating fractals, 2024. (Last accessed on September 2024). 2
- [30] Hongyi Zhang. mixup: Beyond empirical risk minimization. *arXiv preprint arXiv:1710.09412*, 2017. 8
- [31] Richard Zhang, Phillip Isola, Alexei A Efros, Eli Shechtman, and Oliver Wang. The unreasonable effectiveness of deep features as a perceptual metric. In *Proceedings of the IEEE conference on computer vision and pattern recognition*, pages 586–595, 2018. 6
- [32] Yuxin Zhang, Nisha Huang, Fan Tang, Haibin Huang, Chongyang Ma, Weiming Dong, and Changsheng Xu. Inversion-based style transfer with diffusion models. In *Proceedings of the IEEE/CVF conference on computer vision and pattern recognition*, pages 10146–10156, 2023. 3
- [33] Bolei Zhou, Agata Lapedriza, Aditya Khosla, Aude Oliva, and Antonio Torralba. Places: A 10 million image database for scene recognition. *IEEE transactions on pattern analysis and machine intelligence*, 40(6):1452–1464, 2017. 2

# Stylized Structural Patterns for Improved Neural Network Pre-training

## Supplementary Material

### 7. Neural Fractal Generation

In this section, we provide the pseudocode for the coloring and adaptive sampling algorithms.

---

**Algorithm 1:** Dynamic Threshold Adjustment

---

**Input:**  $z$  (first pass data from the rendering),  $ratio$  (desired proportion),  $\tau_{init}$  (initial threshold)

**Initialization:**

- $\tau \leftarrow \tau_{init}$   $\triangleright$  Initialize threshold
- $mask \leftarrow |z| \geq \tau$   $\triangleright$  Create a binary mask for values above threshold

**while**  $average(mask) > ratio$  **do**

- $\tau \leftarrow \tau \times 1.1$   $\triangleright$  Increase threshold
- $mask \leftarrow |z| \geq \tau$   $\triangleright$  Recompute mask

**return**  $\tau$   $\triangleright$  Final threshold

---

---

**Algorithm 2:** Escape Time Coloring Algorithm

---

**Input:**  $max\_iters$ ,  $threshold$ ,  $color\_map$  and a complex network  $g$

**Input:** Sampled coordinate  $c$  from the imageplane

**Output:** Color value of the sampled point

**Initialization:**

- $z \leftarrow 0$
- $i \leftarrow -1$

**while**  $|z| \leq threshold$  **and**  $i < max\_iters$  **do**

- $z \leftarrow g(z) + c$   $\triangleright g(z)$  is the neural network
- $i \leftarrow i + 1$

$T_{esc} \leftarrow i$   $\triangleright T_{esc}$  is the escape time

**if**  $T_{esc} == 0$  **then**

- $T_{esc} \leftarrow max\_iters$

$T_{esc} \leftarrow T_{esc}/max\_iters$

$color \leftarrow color\_map[\text{len}(color\_map) * T_{esc}]$

**return**  $color$

---

### 8. Hyperparameters

**AutoEncoder:** We train the stable diffusion autoencoder (AE) following the hyperparameters in [1]. The latent space of AE has 4 channels as in [1]. We train the AE with images of resolution  $128 \times 128$  and a batch size of 8. We use the Adam optimizer with the learning rate of  $4.5 \times 10^{-6}$ . We train the networks for 1.5M iterations.

**DINO:** We train a ViT-S encoder with DINO pipeline with a batch size of 512 for 200 epochs. The ADAM optimizer is used with a learning rate of 0.0005 with a linear warmup phase lasting 10 epochs. The target learning rate at

---

**Algorithm 3:** Adaptive Sampling Algorithm

---

**Input:**  $max\_epochs$ ,  $max\_iters$ ,  $initial\_samples\_per\_pixel$ , Number of pixels  $n$

**Output:** Color value of the the image plane

**Initialization:**

- $\mu = 0 \forall pixels$   $\triangleright \mu$ : sample mean
- $N = 0 \forall pixels$   $\triangleright N$ : samples per pixel
- $M_2 = 0 \forall pixels$   $\triangleright M_2$ : second moment

**for**  $i = 1$  **to**  $initial\_samples\_per\_pixel$  **do**

- Sample  $C = [c_1, \dots, c_n]$  for each pixel
- $image = get\_color(C)$   $\triangleright$  Use the escape time algorithm
- $\mu = \mu + image$
- $M_2 = M_2 + image^2$
- $N \leftarrow N + 1$

**for**  $i = 1$  **to**  $max\_epochs$  **do**

- $V = M_2/N - (\mu/N)^2$   $\triangleright$  Sample variance per pixel
- $V_m = V/N$   $\triangleright$  Variance of mean per pixel
- $CV_2 = \frac{V}{(\mu/N)^2}$   $\triangleright$  Squared coefficient of variance per pixel
- $CV_2 \leftarrow$  average  $CV_2$  over RGB channels
- $CV_2 \leftarrow box\_blur(CV_2)$
- $S \leftarrow CV_2/\text{sum}(CV_2)$   $\triangleright$  Sampling map

**for**  $j = 1$  **to**  $n$  **do**

- Sample a pixel  $p_j$  from  $S$
- Sample a coordinate  $c_j$  inside  $p_j$  uniformly
- $cr = get\_color(c_j)$
- $\mu(p_j) = \mu(p_j) + cr$
- $M_2(p_j) = M_2(p_j) + cr^2$
- $N(p_j) \leftarrow N(p_j) + 1$

**return**  $\mu/N$

---

the end of optimization is  $10^{-6}$ , following a cosine learning rate schedule. For weight decay (WD), we start with a value of 0.04 and increase it to a final value of 0.4 using a cosine schedule. As suggested in DINO, employing a larger weight decay towards the end of training enhances the performance of ViT-S. After training the ViT-S encoder, we train a single fully connected layer to map its outputs to the classes. We train this layer for 100 epochs, and with Adam optimizer with learning rate 0.0001 and momentum 0.9. We also use cosine annealing learning rate.

**Diffusion:** We use the EDM2-xs architecture from [17]. Karras et al. improved the denoising U-net to converge faster and achieve better results. We pretrain the network

using a batch size of 256 for 840K iterations. We use the Adam optimizer with the learning rate 0.001. We use the same learning rate decay in [17] with  $T_{ref} = 35000$ . Dropout is not applied, and the original noise scheduler remains unchanged. The Flowers dataset is relatively small, having approximately 8K images. As a result, prolonged training leads to overfitting. Therefore, we fine-tune the model for 16K iterations to avoid this problem. In contrast, FFHQ is a larger dataset, containing 70K images. For this setup, we fine-tune the model for 100K iterations.

## 9. Additional Results

**Impact of Network Architecture on Neural Fractal:** We experiment with networks of varying complexity for neural fractal generation. Increasing the complexity of the network tends to increase the frequency of the output image (see Figure 8), making rendering more challenging as low-level details require more samples. Additionally, calling a more complex network slows down generation. To balance rendering speed and image richness, we use a network with 3 layers and 6 neurons. In Figure 8, we present uncurated samples from three networks with 1, 3, and 6 hidden layers.

**Reverse Stylization with the Gatys Algorithm:** The images shown in Figure 10 are reverse-stylized synthetic images generated using the Gatys algorithm.

**Performance of Synthetic Datasets in the Autoencoder Experiment:** Below, we provide some additional figures that summarize and compare the performance of the different datasets that we experiment with. Figure 11 compares the performance of different synthetic datasets in the autoencoder experiment. We observe that non-stylized neural fractal outperforms other non-stylized synthetic datasets. Additionally, we find that stylization improves the accuracy of all base synthetic datasets. In this experiment, the *Gatys* stylization method performs better than *NNST*. Among the stylized datasets, neural fractal once again outperforms the others, achieving the lowest reconstruction error.

**Performance of Synthetic Datasets in the Contrastive Learning Experiment:** Figure 12 presents the results of the contrastive learning experiment using DINO [9]. DINO is a modern and expressive architecture designed for unsupervised settings, offering greater flexibility and performance. In this experiment, neural fractal achieves higher accuracy with and without stylization. The *NNST* stylization method outperforms *Gatys* in this setup.

**Performance of Synthetic Datasets in the Diffusion Experiment:** Figure 13 presents the results of the diffusion experiment on the FFHQ dataset. In this experiment, pretraining with neural fractal achieves the lowest FID after fine-tuning. Stylization further enhances the performance of the neural fractal dataset. Although we did not conduct experiments with other stylized synthetic datasets, we expect similar improvements with stylization. We also evaluate the

1M version of the neural fractal dataset, which consists of 1 million images, and observe that stylization again leads to better performance. Figure 14 shows the results of the diffusion experiment on the Flowers dataset, where a similar trend is observed. Figure 16 and Figure 15 present an uncurated set of generated samples. All models were initialized with the same random number generation seed.

**Latent Space Visualizations of Autoencoders Trained on Different Synthetic Datasets:** To further understand the impact of different training datasets on the learned representations of autoencoders, we visualize the latent spaces in Figure 17. This figure presents the latent representations of samples from the FFHQ and Flowers dataset. For each sample, we display the latent visualizations produced by autoencoders trained on eight different datasets: the input image, ImageNet-100k, VisualAtom, Mandelbulb, FractalDB, StyleGAN, neural fractal (non-stylized), and Stylized Neural Fractal. Upon examining the visualizations, it is evident that the latent representations of the Stylized Neural Fractal are most similar to those of the autoencoder trained on ImageNet-100k. Both exhibit a balanced level of structural detail and noise, unlike some other datasets where the latents appear either excessively noisy (e.g., StyleGAN) or overly structured (e.g., Mandelbulb). This similarity suggests that the stylization process effectively reduces the domain gap between the synthetic neural fractal dataset and real-world data, as represented by ImageNet-100k. While the presence of noise or clear structure in the latents is observable, we refrain from drawing conclusions about their quality or utility based solely on this visualization, as such properties are more directly tied to reconstruction performance (discussed in the main paper, e.g., reconstruction loss metrics). Instead, the key takeaway is that the reduced domain gap between Stylized Neural Fractal and ImageNet-100k may contribute to the improved performance observed in our experiments, highlighting the effectiveness of stylization in aligning synthetic and real data distributions.

**Measuring Distributional Distance between Synthetic and Real Datasets:** We analyze the domain gap between our reverse-stylized Neural Fractals and real data by measuring both distribution-level and network-level similarities. The rightmost column of Table 10 reports the Kernel Inception Distance (KID) and Fréchet Inception Distance (FID) between each synthetic dataset and ImageNet, quantifying how closely their distributions align. KID is particularly robust in high-divergence regimes due to its unbiased estimation and ability to report confidence intervals. To compute KID, we use 100K images and 100 subsets; for FID, we use 50K images. Neural fractal achieves the lowest KID and FID scores, indicating the smallest domain gap and best alignment with real data distributions.

Beyond distributional similarity, we compare how networks trained on different datasets attend to visual features

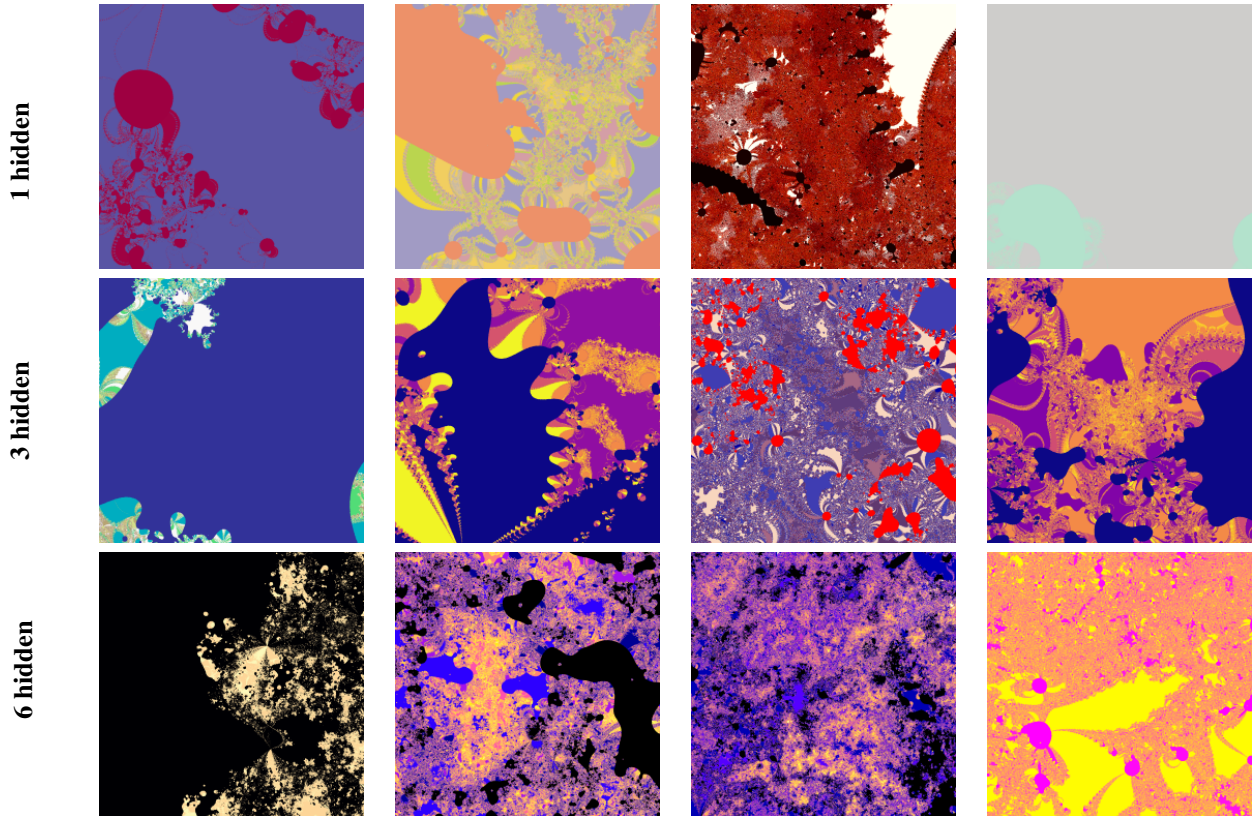


Figure 8. Uncurated samples generated from networks with 1, 3, and 6 hidden layers. The network with 6 hidden layers are more likely to generate images with excessively high frequencies.

Synthetic dataset	ImageNet		COCO	
	<i>Gatys</i>	<i>NNST</i>	<i>Gatys</i>	<i>NNST</i>
VisualAtom	0.111 (+65%)	0.126 (+61%)	0.087 (+71%)	0.102 (+66%)
Mandelbulb	0.115 (+81%)	0.130 (+79%)	0.100 (+80%)	0.117 (+77%)
FractalDB-composite	<u>0.106</u> (+53%)	<u>0.112</u> (+50%)	<b>0.084</b> (+57%)	<u>0.089</u> (+54%)
StyleGAN-oriented	0.107 (+22%)	0.112 (+19%)	<b>0.084</b> (+26%)	<u>0.089</u> (+22%)
Neural Fractals	<b>0.105</b> (+23%)	<b>0.111</b> (+19%)	<b>0.084</b> (+28%)	<b>0.088</b> (+23%)

Table 8. Performance comparison of our stylized synthetic datasets for Autoencoder reconstruction loss, where the Autoencoder is trained on synthetic datasets and evaluated on ImageNet and COCO. Improvements are calculated over the corresponding non-stylized synthetic baseline \* from Table 2,  $\text{improvement} = 100 - 100 \times \frac{\text{stylized}}{\text{nonStylized}}$ . Reverse stylization improves all synthetic datasets. We also see that *Gatys* datasets outperform *NNST* datasets, with neural fractals datasets remaining the best even after stylization, closely followed by our reverse stylized versions of FractalDB-composite and StyleGAN-oriented.

by calculating the cosine similarity of attention maps. The first two columns of Table 10 show this similarity for the autoencoder (left) and the diffusion model (middle), both using ImageNet-100k as the reference. Neural fractal consistently achieves the highest attention map similarity, suggesting that networks trained on it behave most similarly to those trained on ImageNet.

Synthetic dataset	ImageNet-100		Flowers		Food101	
	<i>Gatys</i>	<i>NNST</i>	<i>Gatys</i>	<i>NNST</i>	<i>Gatys</i>	<i>NNST</i>
VisualAtom	55.6 (+17%)	55.8 (+17%)	65.4 (+29%)	68.1 (+32%)	51.7 (+27%)	50.7 (+26%)
Mandelbulb	56.8 (+13%)	57.1 (+13%)	63.6 (+13%)	66.7 (+17%)	52.6 (+12%)	54.0 (+13%)
FractalDB-composite	56.1 (+11%)	57.8 (+13%)	67.5 (+12%)	70.2 (+15%)	52.9 (+16%)	54.3 (+17%)
StyleGAN-oriented	55.9 (+8%)	58.9 (+11%)	68.1 (+20%)	70.7 (+23%)	52.7 (+7%)	54.5 (+9%)
Neural Fractals	<b>57.4 (+9%)</b>	<b>59.2 (+11%)</b>	<b>68.7 (+8%)</b>	<b>71.3 (+11%)</b>	<b>53.8 (+4%)</b>	<b>55.0 (+5%)</b>

Table 9. Performance comparison of our stylized synthetic datasets for DINO with a ViT-S encoder, where the encoder is trained on synthetic datasets and linear evaluation is performed on ImageNet-100, Flowers and Food, measured in accuracy. Improvements are calculated over the corresponding non-stylized synthetic baseline \* from Table 4. Unlike Table 5 and Table 8, improvement = stylized – nonStylized is used to reflect improvements. Reverse stylization improves all synthetic datasets. We also see that *NNST* datasets outperform *Gatys* datasets (except for VisualAtom), with neural fractals datasets remaining the best after stylization.

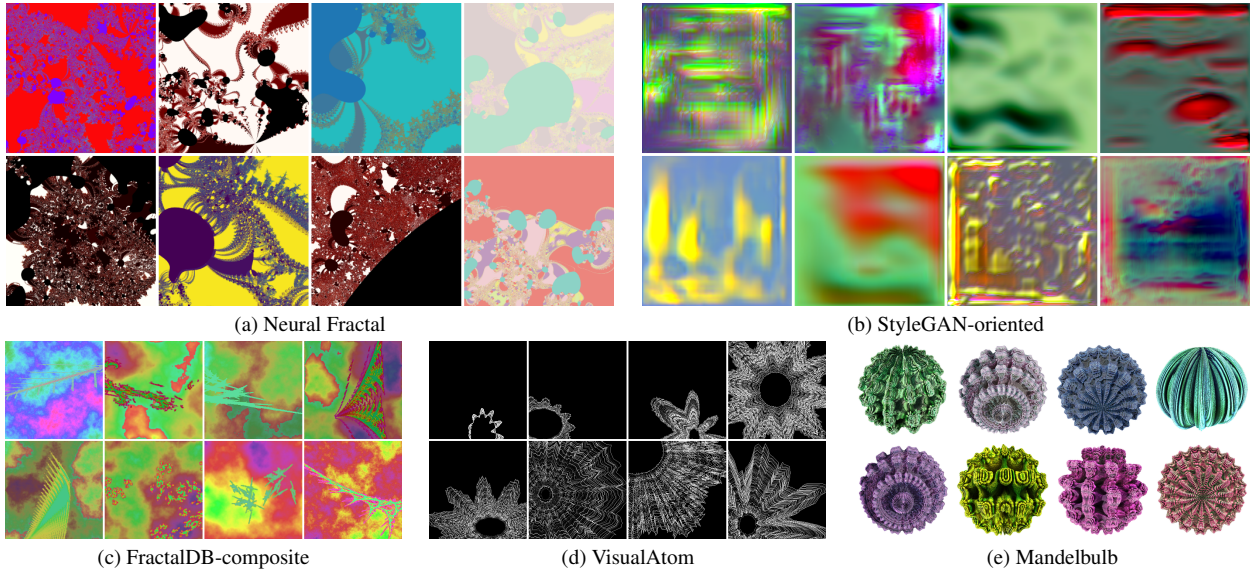


Figure 9. Samples from different base synthetic datasets.

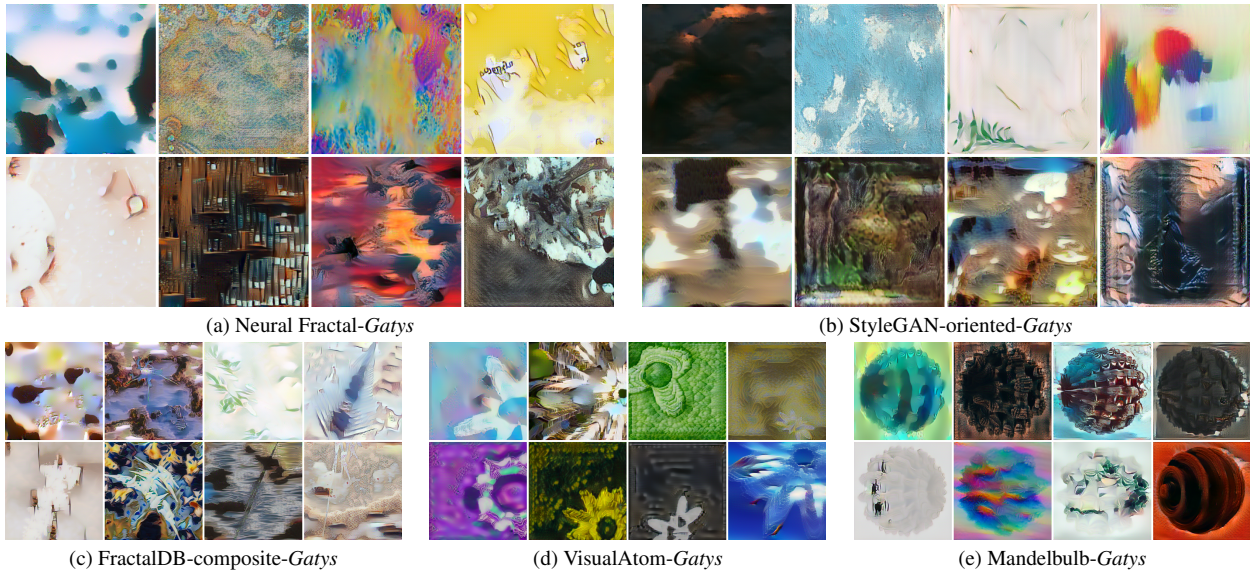


Figure 10. Samples from different *Gatys*-stylized synthetic datasets.

Train/Eval Dataset	AutoEncoding $\uparrow$		ImageGen $\uparrow$	Domain Gap $\downarrow$	
	ImgNet	COCO	ImgNet	KID	FID
VisualAtom	0.28	0.26	0.42	0.203	239.6
Mandelbulb	0.17	0.15	0.35	0.165	211.4
FractalDB-composite	0.50	0.49	0.51	0.214	207.6
StyleGAN-oriented	0.47	0.45	0.54	0.170	193.3
NeuralFractal (ours)	<b>0.55</b>	<b>0.54</b>	<b>0.57</b>	<b>0.162</b>	<b>178.6</b>
+RevStylize (ours)	<b>0.68</b>	<b>0.67</b>	<b>0.61</b>	<b>0.120</b>	<b>148.5</b>

Table 10. The first two columns show cosine similarity between attention maps of a network trained on ImageNet-100 and those trained on synthetic datasets. The left column corresponds to an autoencoder [24] trained for image reconstruction, and the middle column to EDM2 [17] trained with a diffusion loss. Neural fractal achieves the highest cosine similarity, suggesting that neural fractal trained network behaves more similar to the ImageNet trained network. The rightmost column reports two distribution divergence metrics: Kernel Inception Distance (KID) and Fréchet Inception Distance (FID). The metrics are computed between each synthetic dataset and ImageNet, measuring distribution-level similarity. Neural fractal achieves the lowest KID and FID score, indicating the smallest domain gap among all evaluated datasets.

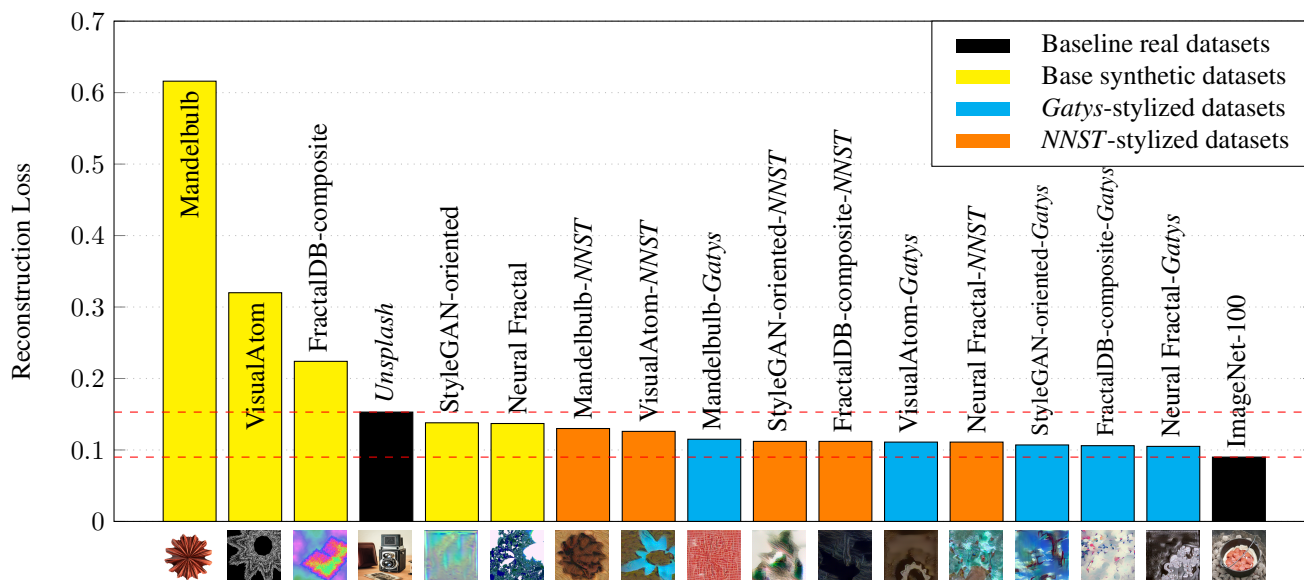


Figure 11. Autoencoder reconstruction loss for different datasets. Datasets are sorted in increasing order by performance along the x-axis. The dashed lines represent the lower and upper bounds in performance that can be achieved using small and large real datasets respectively.

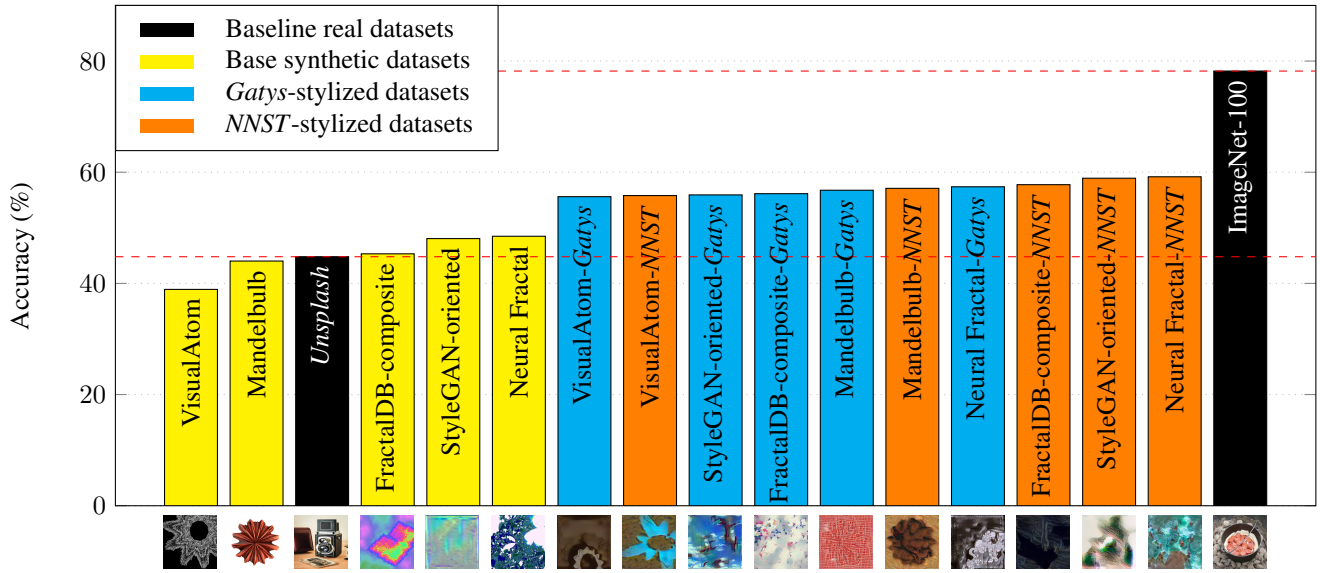


Figure 12. Top-1 accuracy on ImageNet-100 for different datasets evaluated using the DINO-based evaluation pipeline [28]. Datasets are sorted in increasing order by performance along the x-axis. The dashed lines represent the lower and upper bounds in performance that can be achieved using small and large real datasets respectively.

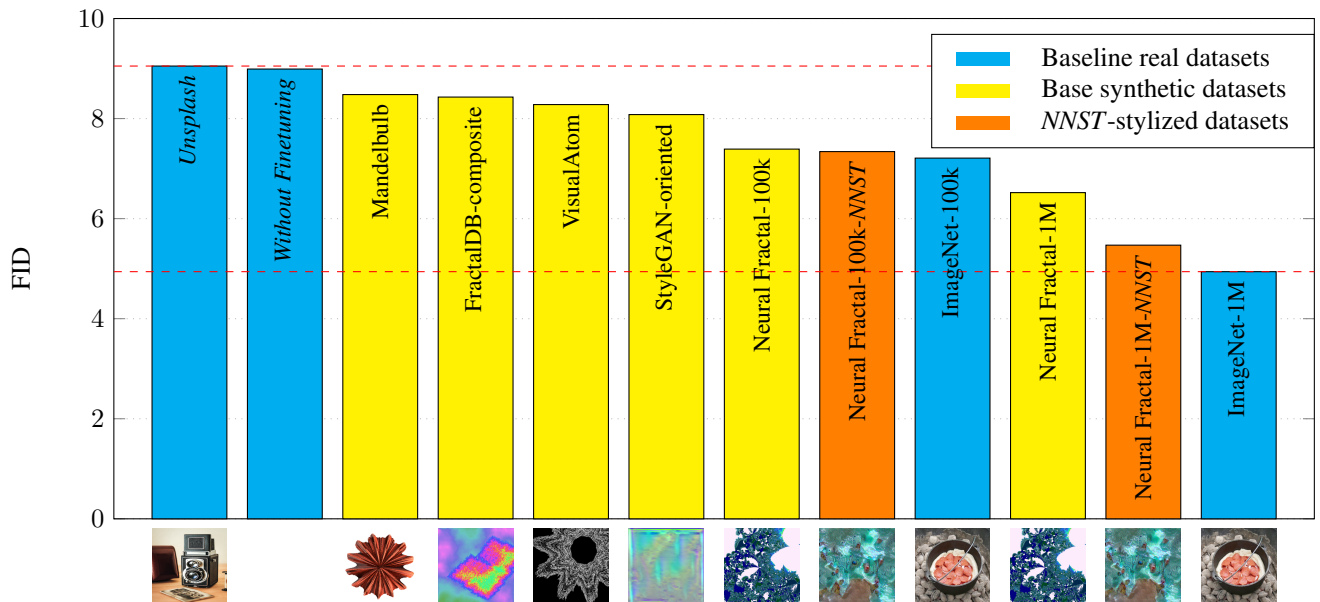


Figure 13. FID scores for models trained on the FFHQ dataset, illustrating the impact of different pretraining datasets. Models are grouped by dataset type: baseline real datasets (blue), base synthetic datasets (yellow), and NNST-stylized datasets (orange). Lower FID scores indicate better performance, with models sorted from highest to lowest FID. Sample images from each dataset are shown below the bars.

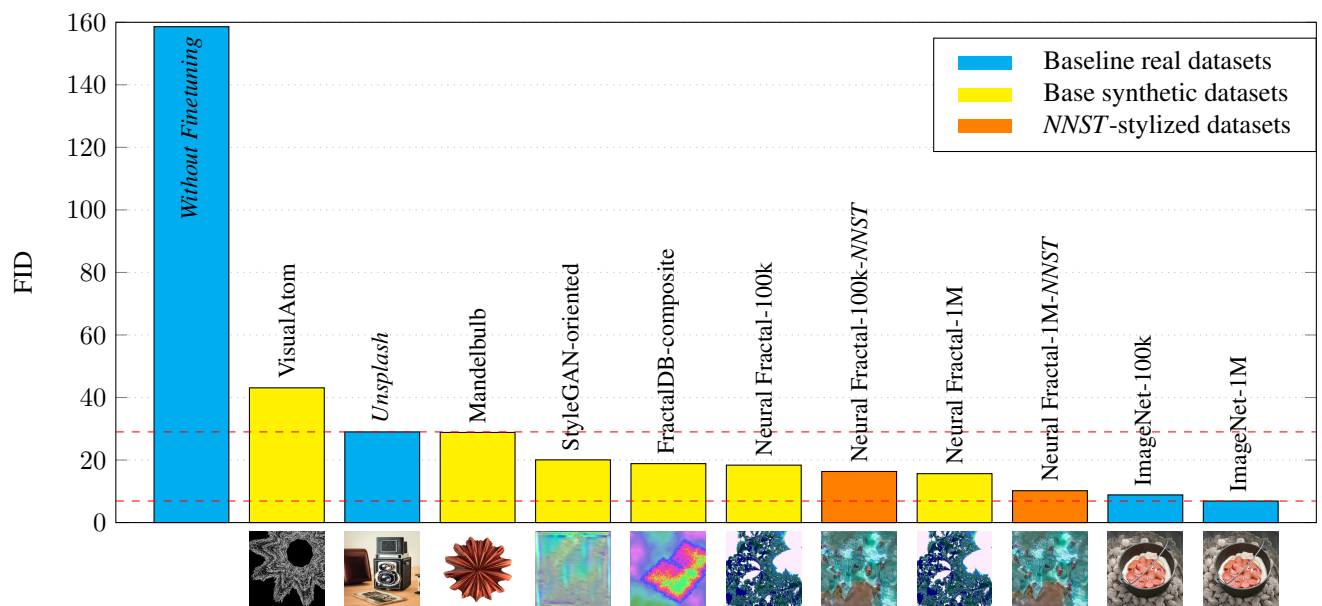


Figure 14. FID scores for models trained on the Flowers dataset, highlighting the influence of different pretraining datasets. Models are categorized into baseline real datasets (blue), base synthetic datasets (yellow), and NNST-stylized datasets (orange). Lower FID scores represent improved performance, with models sorted from highest to lowest FID. Sample images from each dataset are displayed beneath the bars.

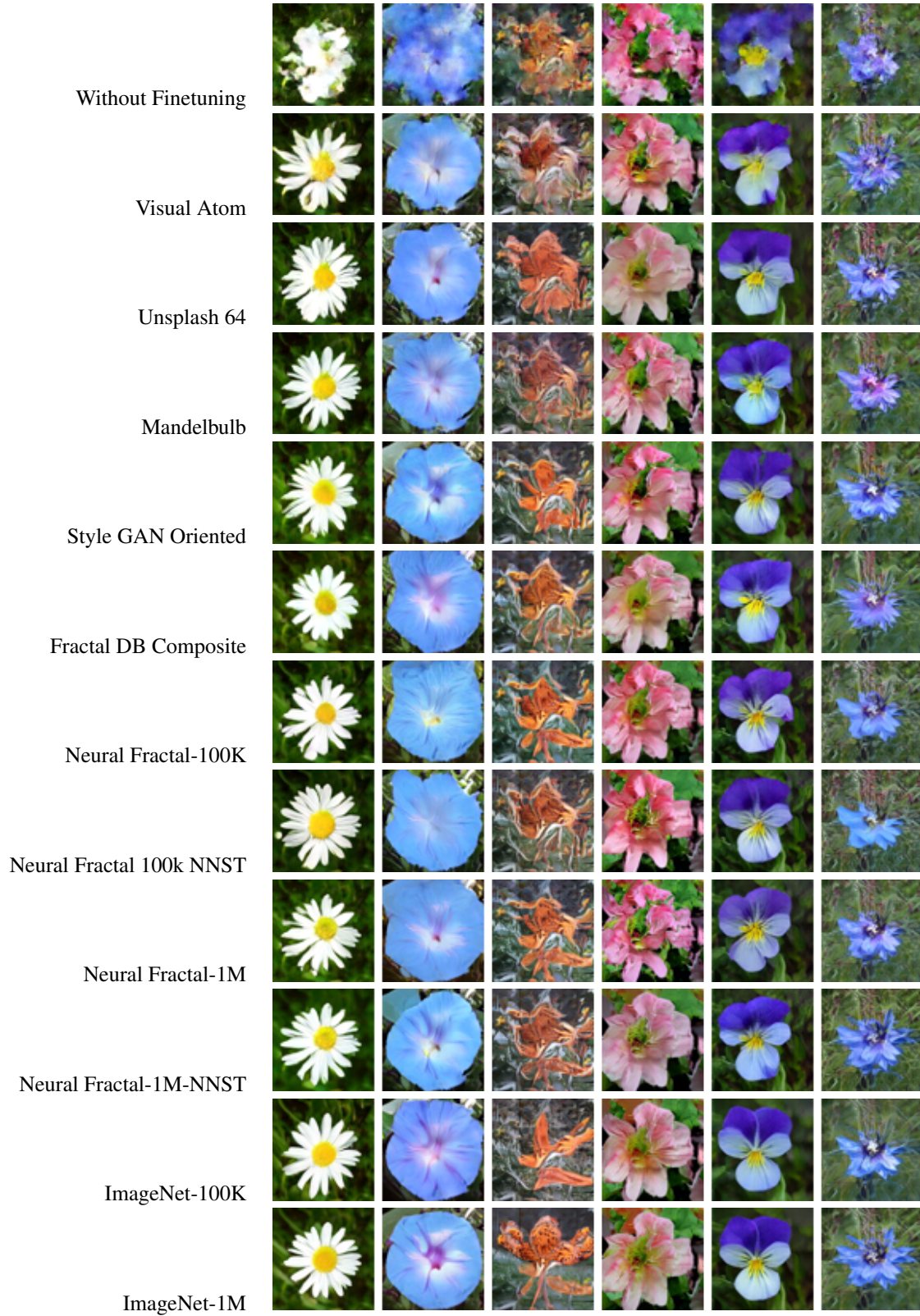


Figure 15. Comparison of sample images generated by different models trained on the Flowers dataset. The models differ in their pretraining datasets. The images are ordered by their FID scores, with the highest FID at the top and the lowest FID at the bottom.

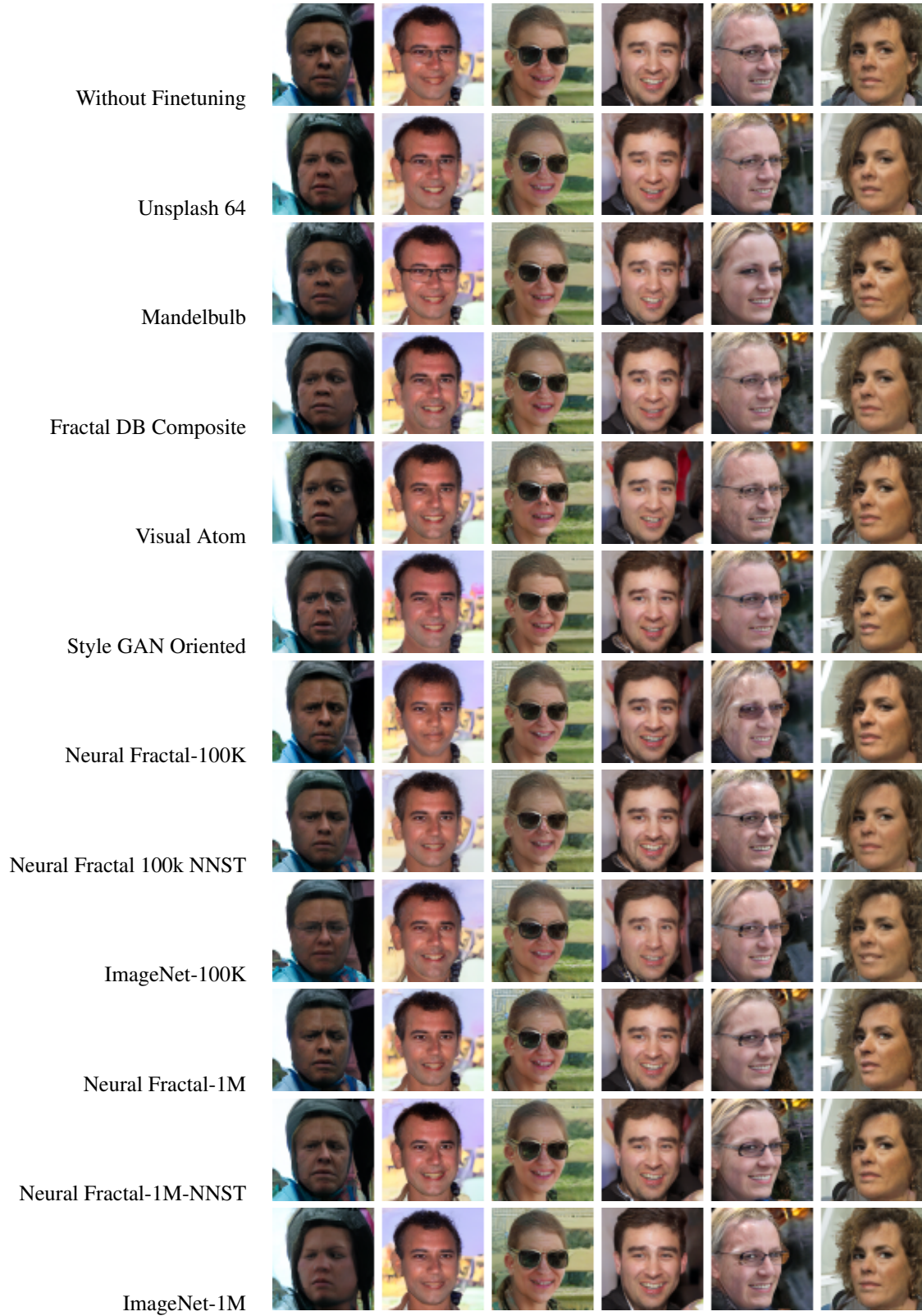


Figure 16. Comparison of sample images generated by different models trained on the FFHQ dataset. The models differ in their pretraining datasets. The images are ordered by their FID scores, with the highest FID at the top and the lowest FID at the bottom.

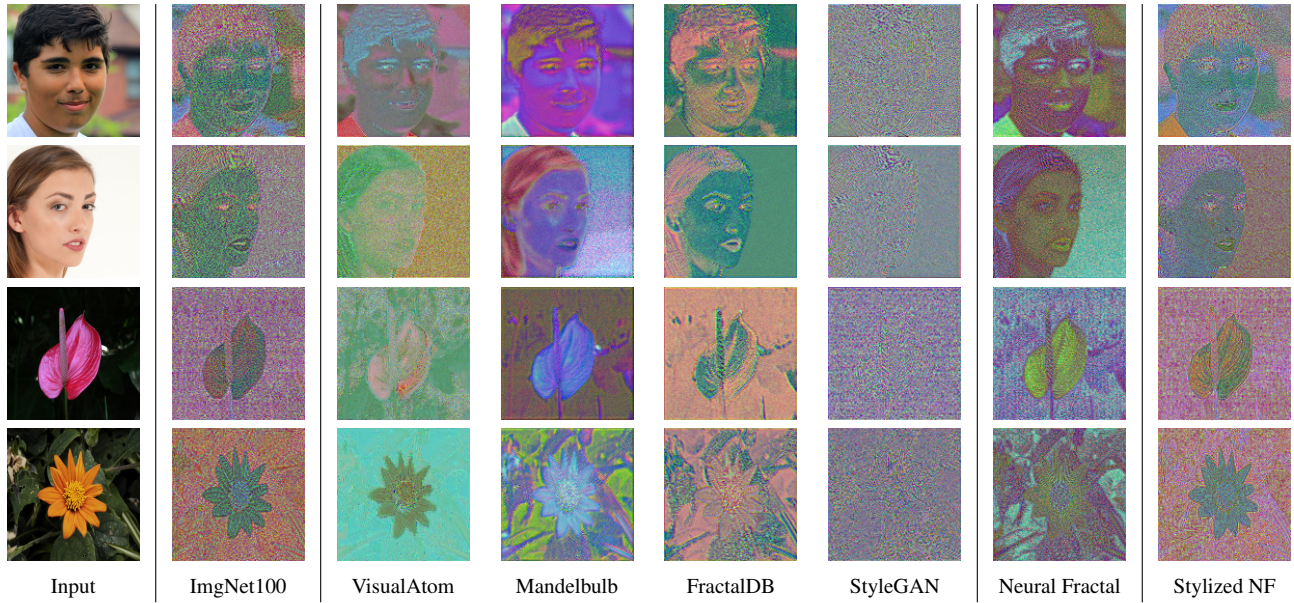


Figure 17. Visualization of latent representations from autoencoders trained on different datasets. The figure consists of samples from FFHQ and Flowers dataset. The similarity between the latents of the Stylized Neural Fractal and ImageNet-100k suggests a reduced domain gap, supporting the effectiveness of the stylization approach.

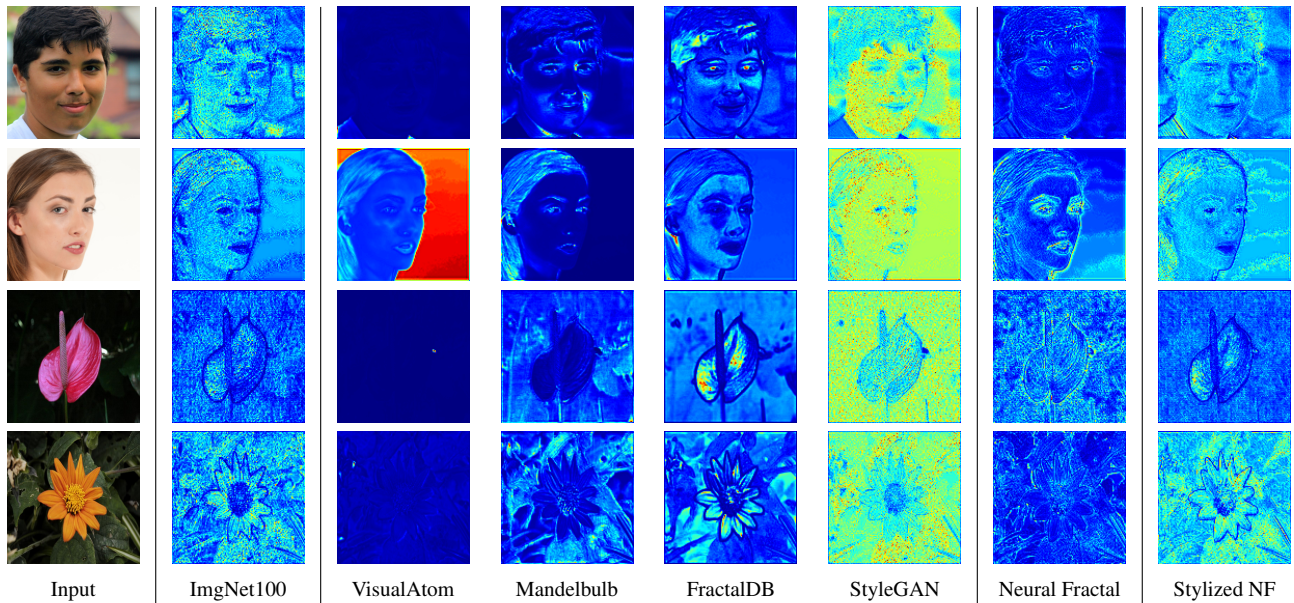


Figure 18. Visualization of attention maps representations from autoencoders trained on different datasets.